Polymer Brushes: From Self-Consistent Field Theory to Classical Theory

Roland R. Netz*,†,‡ and M. Schick†

Department of Physics, University of Washington, Box 351560, Seattle, Washington 98195-1560, and Max-Planck-Institut für Kolloid- und Grenzflächenforschung, Kantstrasse 55, 14513 Teltow, Germany

Received December 2, 1997; Revised Manuscript Received April 9, 1998

ABSTRACT: We consider planar brushes formed by end-grafted polymers with moderate to strong excluded-volume interactions. We first rederive the mean-field theory and solve the resulting self-consistent equations numerically. In the continuum limit, the results depend sensitively on a single parameter, β, whose square is the ratio of the scaling prediction for the brush height to the unperturbed polymer radius of gyration, and which measures therefore the degree to which the polymers are stretched. For large values of β, the density profile is close to parabolic, as predicted by the infinite-stretching theory of Zhulina et al. and of Milner et al. As β decreases, the profile deviates strongly from a parabolic one. By calculating the most probable paths and comparing their contribution to various properties with those obtained from the full self-consistent theory, we determine the effect of the fluctuations about such paths. At large values of β, these effects are very small everywhere. As β decreases, fluctuation effects on the density profile become increasingly important near the grafting surface, but remain small far from it. For all values of β, we find that polymer paths which begin far from the grafting surface are strongly, and almost uniformly, stretched throughout their length, including their free end points. Paths which begin close to the grafting surface are also stretched, but they initially move *away* from the grafting surface before reaching a maximum height and then returning to it. The classical theory is then derived from the self-consistent field equations by retaining, for each end point location, only that single trajectory which minimizes the free energy of the system. This free energy contains an entropy, of relative weight β^{-1}, which arises from the distribution of end points. Even for brushes which are only moderately stretched, the results of the classical theory for the brush profile and polymer end point distribution agree well with those of the full self-consistent theory except near the grafting surface itself. There the density profile as calculated in the self-consistent theory shows a characteristic decrease which is not captured by the classical theory. However it does capture the fact that the individual polymer paths are stretched in general throughout their length, including the end points, and yields nonmonotonic paths for polymers whose end points are close to the grafting surface. In addition, it reproduces extremely well the form of the density distribution far from the grafting surface, which is essentially Gaussian. This results from the fact that the stretching energy dominates the interaction energy of those polymers which extend far from the grafting surface, so that their behavior is nearly ideal. In the limit of infinite stretching, $\beta \to \infty$, the theory reduces to that of Zhulina et al. and of Milner et al.

I. Introduction

At high surface coverage and moderate to strong excluded volume interactions, one finds that polymer chains grafted at one end to a planar surface are strongly stretched, forming a *polymer brush*.[1,2] Such systems have several applications including colloidal stabilization, surface modification, and lubrication. They also serve as a testing ground for theoretical models and approaches due to their conceptual simplicity. After the early work of Alexander[3] and de Gennes,[4] Milner, Witten, and Cates[5] and Zhulina and co-workers[6] developed a theory which took advantage of the fact that in a system in which polymers are strongly stretched, as in a brush, fluctuations around the most probable, or "classical", paths are small, and can be ignored to first approximation.[7] This theory was derived in the limit in which the thickness of the brush is infinitely greater than the unperturbed radius of gyration of the polymers composing it. Therefore the theory is the classical theory *in the infinite-stretching limit*. (We shall refer to it, accordingly, as the ISL theory.) Its predictions include a parabolic form for the monomer-density profile, a polymer end point distribution which is nonzero only within a finite distance from the grafting surface, and a universal form for all classical polymer paths, which are unstretched at their free end, and which differ only in their amplitude.

Since the formulation of the ISL theory, there has been little attempt to derive the classical theory for a brush stretched a *finite*, and arbitrary, amount. Recently an attempt[8] to do so approximately produced a density profile for a strongly, but finitely stretched, system which was in closer agreement with the results of a full self-consistent field theory treatment than was that of the ISL. This indicated that a classical theory might be useful over a range of stretching parameters.

In this article we derive the classical theory for polymer brushes which are stretched a finite, and arbitrary, amount and compare its results with numerical self-consistent field (scf) calculations using continuum techniques analogous to the Scheutjens−Fleer method[9,10] for discrete systems. In the continuum limit, results of both classical and scf theories depend sensitively on a single parameter, β, proportional to the square of the scaling prediction for the brush height to the unperturbed polymer radius of gyration. They have the following qualitative features:[11] (i) the density profile has a tail which, at large distances, is Gaussian,

* To whom correspondence should be addressed at the Max-Planck-Institut für Kolloid- und Grenzflächenforschung.
† University of Washington.
‡ Max-Planck-Institut für Kolloid- und Grenzflächenforschung.

S0024-9297(97)01750-6 CCC: $15.00
Published on Web 06/27/1998

(ii) the end point distribution is nonzero everywhere, (iii) classical paths with different free end point positions are different, (iv) paths whose free end points lie beyond a certain distance from the grafting surface proceed monotonically to the grafting surface and are stretched throughout their entire length, including the end point, and (v) paths whose free end points lie within that distance initially proceed *away* from the grafting surface, reach a maximum, and then continue to the surface. They are stretched everywhere except at the maximum. The limits of both the classical and the scf theories, as the relative brush height diverges, are those of the ISL.[5,6]

The additional component which arises in our classical theory for arbitrary stretching is the entropy associated with the distribution of end points, which has a weight β^{-1}. Therefore the effect of the entropy vanishes in the infinite stretching limit $\beta \to \infty$. Its presence at finite stretching causes the results of our classical theory to differ qualitatively from those of the ISL. Comparison of various quantities as calculated from the classical and the scf theories for finite values of β shows that the main effects of fluctuations about the classical paths occur near the grafting surface itself, in agreement with previous predictions.[12] Entropic repulsions due to the impenetrable wall are missed completely by the classical theory. In contrast, far from the grafting surface, the two theories become equivalent.

In section II, we define the polymeric model we employ to describe the brush, and bring it to an equivalent, but more convenient, form by applying exact transformations which utilize auxiliary fields. In section III, we employ the mean-field, or scf, approximation which results in a set of self-consistent equations that are solved numerically in section IV. Here we also calculate the most probable paths and show how they differ depending upon the location of the end point and the degree to which the brush is stretched, β. We then derive the classical approximation to the scf theory in section V and display some of its results for several values of the stretching parameter. In an appendix, we demonstrate that the ISL of Milner, Witten, and Cates and of Zhulina et al. are obtained in the limit $\beta \to \infty$. Section VI is devoted to a detailed comparison between the classical and scf theories and includes a comparison of individual polymer paths and the behavior far from the grafting surface. We also provide exact results for the scf theory in the limit when the excluded volume interaction vanishes, which illustrates the effect of the impenetrable grafting surface. Density fluctuations are not accounted for in the mean-field theory or the classical theory which derives from it. They are, of course, included in molecular dynamics[13] and Monte Carlo[14−17] simulations. Direct comparison of results is difficult, however, since simulations and scf calculations usually use different microscopic polymer models. The expected effects of fluctuations as obtained from simple scaling ideas and the range of validity of our assumptions are discussed in the final section.

II. The Partition Function for Grafted Polymers

We begin with the partition function for n Gaussian polymers, end-grafted to an area A, which interact via a quadratic repulsion of strength w

$$Z[h]=\frac{1}{n!}\prod_{\alpha=1}^{n}\left[\int D\mathbf{r}_\alpha(\cdot)\exp\left\{-\frac{3}{2a^2}\int_0^N \dot{\mathbf{r}}_\alpha^2(s)\,ds\right\}\right]\times \exp\left\{-\int\frac{w}{2}\hat{\Psi}^2(\mathbf{r})-h(\mathbf{r})\hat{\Psi}(\mathbf{r})\,d\mathbf{r}\right\} \quad (1)$$

where a denotes the Kuhn length, and the monomer density $\hat{\Psi}$ is defined by

$$\hat{\Psi}(\mathbf{r})=\sum_{\alpha=1}^{n}\int_0^N ds\;\delta[\mathbf{r}-\mathbf{r}_\alpha(s)] \quad (2)$$

The circumflex denotes the dependence of the density on all individual polymer configurations. It is implicitly assumed that all polymers end at a planar grafting surface which is impenetrable, so that they are confined to a half-space. The field h acts as a generating field, and will be used to calculate density ensemble averages and correlation functions. The Gaussian expression for the polymer elasticity is, of course, only valid for polymers which are not stretched to their contour length.[18] In the discussion in section VII we will show that the use of the Gaussian elasticity is not a limiting factor in the validity of our results, because the mean-field approximation breaks down before the limit of extreme stretching is reached. More serious is the restriction in eq 1 to the second virial coefficient.[22,23] Higher order terms in the density become important when the system is near the Θ point,[6] and wherever the monomer density is expected to be large, such as the vicinity of the grafting surface. Since we are concerned in this article with the generic features of a classical theory, we leave generalizations of the present model to future activity.

To make the expression for the partition function more tractable, we insert the identity

$$1=\int D\Psi(\cdot)\,\delta[\Psi(\cdot)-\hat{\Psi}(\cdot)] \quad (3)$$

and use the integral representation of the delta function

$$\delta[\Psi(\cdot)-\hat{\Psi}(\cdot)]=\int D\Omega(\cdot)\exp\{\int\Omega(\mathbf{r})[\Psi(\mathbf{r})-\hat{\Psi}(\mathbf{r})]\,d\mathbf{r}\} \quad (4)$$

the functional integral over $\Omega(\cdot)$ is a contour integral along the imaginary axis. In the resulting expression for the partition function, one can carry out the Gaussian integration over $\Psi(\cdot)$. This yields (up to an unimportant multiplicative factor N)

$$Z[h]=\frac{N}{n!}\int D\Omega(\cdot)\exp(-nF[\Omega,h]) \quad (5)$$

with the new functional F defined by

$$F[\Omega,h]=-\frac{1}{2wn}\int(\Omega(\mathbf{r})+h(\mathbf{r}))^2\,d\mathbf{r}-\ln Z[\Omega] \quad (6)$$

where $Q[\Omega]$ is the partition function of a single polymer in an external field Ω

$$Q[\Omega]=\int D\mathbf{r}(\cdot)\exp\left\{-\int_0^N\frac{3}{2a^2}\dot{\mathbf{r}}^2(s)+\Omega[\mathbf{r}(s)]\,ds\right\} \quad (7)$$

To this point, we have made no approximations, and the two expressions for the partition function, eqs 1 and 5, are equivalent. We are also not closer to obtaining the partition function, since to perform the integral over

the fluctuating field $\Omega(\cdot)$ in eq 5 is at least as difficult as the summation over individual polymer paths in eq 1. The reason for rewriting the partition function is that the mean-field approximation can now be implemented in a particularly lucid fashion, and this is done in the next section.

III. Mean-Field Approximation

Mean-field theory is obtained when the functional integral over the field $\Omega(\mathbf{r})$ in the partition function Z, eq 5, is approximated by the integrand evaluated at that value $\omega(\mathbf{r})$ of $\Omega(\mathbf{r})$ which extremizes the functional $F[\Omega]$. The field $\omega(\mathbf{r})$ is therefore determined by the equation

$$\frac{\delta F[\omega,h=0]}{\delta\omega(\mathbf{r})} = -\frac{1}{wn}\omega(\mathbf{r}) - \frac{\delta \ln Q[\omega]}{\delta\omega(\mathbf{r})} = 0 \qquad (8)$$

The mean-field approximation to the free energy per polymer, F_{mf}, is simply

$$F_{\mathrm{mf}} \equiv F[\omega,h=0] \qquad (9)$$

Note that we do not include the entropy of ideal mixing coming from the factor 1/n! in the free energy expression. The density distribution within the mean-field approximation, denoted by $\psi(\mathbf{r})$, is given by

$$\psi(\mathbf{r}) \equiv \langle\Psi(\mathbf{r})\rangle_{\mathrm{mf}} = -n\frac{\delta F[\omega,h]}{\delta h(\mathbf{r})}|_{h(\cdot)=0} = \frac{\omega(\mathbf{r})}{w} \qquad (10)$$

and thus is proportional to the extremal field $\omega(\mathbf{r})$. In order to estimate to what extent fluctuations are taken into account, we calculate the connected correlation function

$$\langle\Psi(\mathbf{r})\Psi(\mathbf{r}')\rangle_{\mathrm{mf}} - \langle\Psi(\mathbf{r})\rangle_{\mathrm{mf}}{}^2 = -n\frac{\delta^2 F[\omega,h]}{\delta h(\mathbf{r})\delta h(\mathbf{r}')}|_{h(\cdot)=0} = \frac{\delta(\mathbf{r}-\mathbf{r}')}{w}$$

This shows that, by approximating the integral over Ω in eq 5 by the extremal value of the integrand, we include density fluctuations on a Gaussian level, but miss correlations completely, as expected in the mean-field approximation. Also note that all higher correlation functions are identically zero and that the susceptibility, obtained by integrating over the connected two-point correlation function, yields the expected mean-field scaling $\sim 1/w$. The effects of correlations, and the range of parameters over which they are anticipated to be unimportant, are discussed in section VII. In the next section, we proceed to a simple limit in which fluctuations of the auxiliary field Ω can in fact be neglected.

Because the density $\psi(\mathbf{r})$ is a real function, the extremum of F (defined in eq 6) with respect to Ω lies on the real axis. As the integrand in eq 5 contains no poles in the complex plane of Ω, we can distort the integration contour so that it passes through this extremum. By virtue of the Cauchy−Riemann conditions, we know that the extremum is in fact a saddle point, which justifies the equivalent notation for this simplification, *saddle point approximation*. The functional $F[\Omega]$ shows a minimum at the saddle point as Ω is varied along the imaginary axis, but it is a maximum with respect to variation along the real axis.

By combining eqs 8 and 10, we can rewrite the self-consistent equation which stands at the heart of the mean-field approximation as

$$\psi(\mathbf{r}) = -n\frac{\delta \ln Q[w\psi]}{\delta w\psi(\mathbf{r})} \qquad (11)$$

and the mean-field free energy per polymer

$$F_{\mathrm{mf}} = -\frac{w}{2n}\int \mathrm{d}\mathbf{r}\ \psi^2(\mathbf{r}) - \ln Q[w\psi] \qquad (12)$$

The mean-field approximation, which consists of neglecting the spatial correlations of the density, is expected to be accurate when each chain interacts locally with many other chains, i.e., when the polymer concentration is higher than that at which chains just begin to overlap. It follows that fluctuation effects might become important somewhere near the edge of the brush because the density decreases to zero continuously and must drop below the overlap concentration as it does so. This point will be investigated further in the discussion at the end of this article. We will show that very far away from the grafting surface mean-field theory should become accurate again, because the excluded-volume interaction becomes irrelevant for highly-stretched polymers.

We now show that mean-field theory is exact if one can neglect lateral variations of the density. If so, the density becomes a function only of the distance from the wall, denoted by $r_\perp$. To make the discussion more transparent, we introduce the dimensionless coordinate $z = r_\perp/\hat{z}$, where $\hat{z}$ is the length scale of the extent of the brush according to the scaling and Flory theories[3,4]

$$\hat{z} \equiv N(2w\sigma a^2/3)^{1/3} \qquad (13)$$

with $\sigma \equiv n/A$ being the grafting density, and we also introduce a dimensionless, rescaled, density

$$\Phi(z) \equiv \Psi(z\hat{z})\hat{z}/(N\sigma) \qquad (14)$$

This dimensionless density satisfies the normalization condition

$$\int_0^\infty \Phi(z)\,\mathrm{d}z = 1 \qquad (15)$$

as follows from the definition of the monomer density, eq 2. Using the fact that the density does not depend on the lateral coordinates, we can rewrite the exact partition function, eq 5, with h set to zero as

$$Z = \frac{N}{\mathrm{n!}}\int D\Phi(\cdot)\,\exp(-nF[\Phi]) \qquad (16)$$

The free-energy functional, eq 6, expressed in terms of the dimensionless density is given by

$$F[\Phi] = -\frac{\beta}{2}\int \Phi(z)^2\,\mathrm{d}z - \ln Q[\Phi] \qquad (17)$$

with the single-polymer partition function

$$Q[\Phi] = \int_0^\infty Dz(\cdot)\,\exp\{-\beta\int_0^1 \dot{z}^2(t) + \Phi[z(t)]\mathrm{d}t\} \qquad (18)$$

Note that the internal polymer coordinate has been rescaled by a factor of N, so that the integration along the polymer contour now runs from zero to one. The only parameter remaining in the theory is

$$\beta \equiv N\left(\frac{3w^2\sigma^2}{2a^2}\right)^{1/3} = \frac{3}{2}\left(\frac{\hat{z}}{N^{1/2}a}\right)^2 \qquad (19)$$

which is the square of the ratio of the typical length scale $\hat{z}$ to the polymer radius of gyration $aN^{1/2}$. As our results demonstrate, the actual brush height is on the order of $\hat{z}$ only for large values of β, in which case β is a direct measure of the extent to which the polymers in the brush are stretched. For values of β smaller than unity, the brush height is on the order of the radius of gyration and thus is much larger than the length scale $\hat{z}$.

The self-consistent equation determining the rescaled mean-field density $\phi(z)$ is

$$\phi(z) = -\frac{\delta \ln Q[\phi]}{\delta\beta\phi(z)} \tag{20}$$

and the mean field free energy is

$$F_{\mathrm{mf}} = -\frac{\beta}{2}\int \phi(z)^2\,\mathrm{d}z - \ln Q[\phi] \tag{21}$$

The functional integral in the partition function, eq 16, involves a fluctuating field which only depends on one coordinate, the distance from the grafting wall. By expanding the functional $F[\Phi]$ around the saddle point $\phi(\cdot)$ up to second order and performing the Gaussian integration over $\Phi(\cdot)$, we see that the free energy per polymer, including Gaussian fluctuations, is given by the mean-field free energy, eq 21, plus corrections which are proportional to $(\ln n)/n$. These corrections vanish in the thermodynamic limit $n \to \infty$, so that the mean-field free energy is exact.[24] Thus, if there are no fluctuations in the density parallel to the grafting surface, then there are no fluctuations in the density perpendicular to it. The latter will only occur in a theory which permits lateral density fluctuations.

IV. Numerical Solution of the Self-Consistent Equation

Numerical solutions of the self-consistent equations have been obtained several times[9,10,14,25,26] using the methods of Scheutjens and Fleer. What has not been done before, and which we do here, is to examine the most probable polymer trajectories both as a function of their starting position, z_0, and the degree of stretching of the brush, β, in which they are embedded. The results of this section show that the most probable polymer paths for a brush which is stretched a finite amount can be very different from those predicted by the ISL theory. They also clarify the salient features of these paths. The ability of a classical theory to reproduce these features is one measure by which it can be judged.

To solve numerically the self-consistent eq 20 in the continuum limit, one introduces the segment probability amplitudes

$$q(z,t) = \int_0^\infty \mathcal{D}z(\cdot)\delta[z(t) - z]\exp\{-\beta\int_0^t \dot{z}^2(t') + \phi[z(t')]\,\mathrm{d}t'\} \tag{22}$$

$$q^\dagger(z,t) = \int_0^\infty \mathcal{D}z(\cdot)\delta[z(t) - z]\exp\{-\beta\int_t^1 \dot{z}^2(t') + \phi[z(t')]\,\mathrm{d}t'\} \tag{23}$$

which depend on the density distribution $\phi(z)$. These amplitudes can be viewed as the polymer propagators, or Green's function, along the internal polymer coordinate and opposite to it, respectively. Note that the internal coordinate t is defined such that its values at the free and at the grafted ends are zero and unity respectively. The initial conditions are $q(z,0) = 1$,[27] meaning that the initial propagator of the ungrafted polymer ends is unbiased, and $q^\dagger(z,1) = \delta(z)$, meaning that all polymers end at the grafting surface. The unnormalized probability to find the polymer segment t at position z is given by $q(z,t)q^\dagger(z,t)$. Clearly, the single polymer partition function is given by

$$Q[\phi] = \int_0^\infty \mathrm{d}z\; q(z,t)q^\dagger(z,t) \tag{24}$$

and is independent of t. Using this relation and the equation of self-consistency, eq 20, we can write the polymer density as

$$\phi(z) = \frac{1}{Q}\int_0^1 \mathrm{d}t\; q(z,t)q^\dagger(z,t) \tag{25}$$

Self-consistency now demands that the density calculated via eq 25 be equal to the density used to evaluate the segment amplitude distributions via eqs 22 and 23. Numerically, this can easily be achieved by some linear relaxation algorithm.

In the numerical solution, one has to discretize both the time coordinate t and the spatial coordinate z. The discretization of the time coordinate is not critical, and we found $M_t = 100$ discretization points to be sufficient. The spatial discretization is more sensitive. Denoting the number of spatial discretization points per unit length by M_z, we find that the Gaussian distribution of the discretized Green's functions is well represented if M_z satisfies $M_z > 10(\beta M_t)^{1/2}$. As we checked explicitly, the solutions then correspond to the continuum limit in every respect. The box size was always chosen large enough so that boundary effects were negligible.

Our derivation of the self-consistent equations, eqs 22, 23, and 25, is similar to the calculations in refs 9, 10, 14, 25, 26. In order to be able to compare the numerical results with the predictions of the classical theory, we evaluate the self-consistent equations in the continuum limit, in contrast to the above-cited references. In previous numerical work, the polymer was assumed to perform a so-called restricted random walk, such that neighboring polymer segments can only change their vertical position by one lattice unit at most.

Figure 1a shows our results for the density profile, $\phi(z)$, for four different values of β: 100 (solid line), 10 (dashed line), 1 (dashed−dotted line), and 0.1 (dotted line). The bold dashed line denotes the parabolic prediction of the ISL of Milner, Witten, Cates, and Zhulina et al. While the density distributions of the scf theory are close to parabolic for large β, they deviate from this form considerably as β decreases, becoming progressively flatter. The impenetrable hard wall causes a depression in the density close to the grafting surface, and pushes the density maximum away from the wall; this effect has been extensively discussed in previous calculations.[9,10,14,25,26] The density maximum moves further away from the wall as β decreases (the results are replotted on an extended scale in Figure 6).

Figure 1b shows the normalized end-point distribution $g(z)$, which is given by

$$g(z) = \frac{q^\dagger(z,0)}{Q} \tag{26}$$

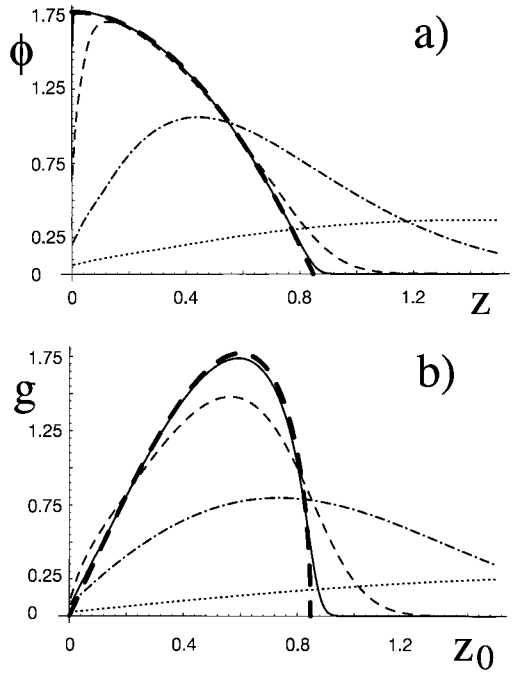

Figure 1. (a) Self-consistent-field (scf) results for the (a) rescaled density profiles ϕ as a function of the rescaled distance z from the grafting surface. Shown are results for $\beta = 0.1$, 1, 10, and 100 (dotted, dash−dotted, dashed, and solid lines, respectively), progressively approaching the asymptotic result (valid for $\beta \to \infty$), shown as a thick dashed line. (b) Rescaled end-point distribution g as a function of the end-point position z_0. The results are for the same values of β as in part a and again approach the asymptotic result (thick dashed line).

(Note that, according to common usage, we have defined the internal coordinate of the polymers to begin at the free end.) Again, the results for $\beta = 100$ (solid line) agree well with the predictions of the ISL (heavy dashed line), but deviations become more pronounced as β decreases (the data are replotted on an extended scale in Figure 7). Needless to say, the end-point distribution is nonzero everywhere, however small it might become as one moves away from the grafting surface. The asymptotic behavior of both the monomer density and the end-point distribution will be investigated further in section VI.

To gain a better understanding of the statistics of individual polymers, we calculate polymer paths with constrained starting points. To carry out these calculations, we define a conditional segment distribution function $q(z,t)|_{z_0}$, which is given by eq 22, but with the modified initial condition $q(z,0) = \delta[z - z_0]$, so that one considers only polymers starting at a height z_0. The conditional, normalized, probability to find at height z a segment with the internal coordinate t of a polymer which starts at a height z_0 is given by

$$P(z,t)|_{z_0} = \frac{q(z,t)|_{z_0} q^{\dagger}(z,t)}{\int_0^{\infty} dz'\, q(z',t)|_{z_0} q^{\dagger}(z',t)} \qquad (27)$$

The maximum of this function defines the most probable path of a polymer which starts at z_0. The average path of a polymer starting at z_0 is

$$\langle z(t)|_{z_0} \rangle = \int_0^{\infty} z P(z,t)|_{z_0}\, dz \qquad (28)$$

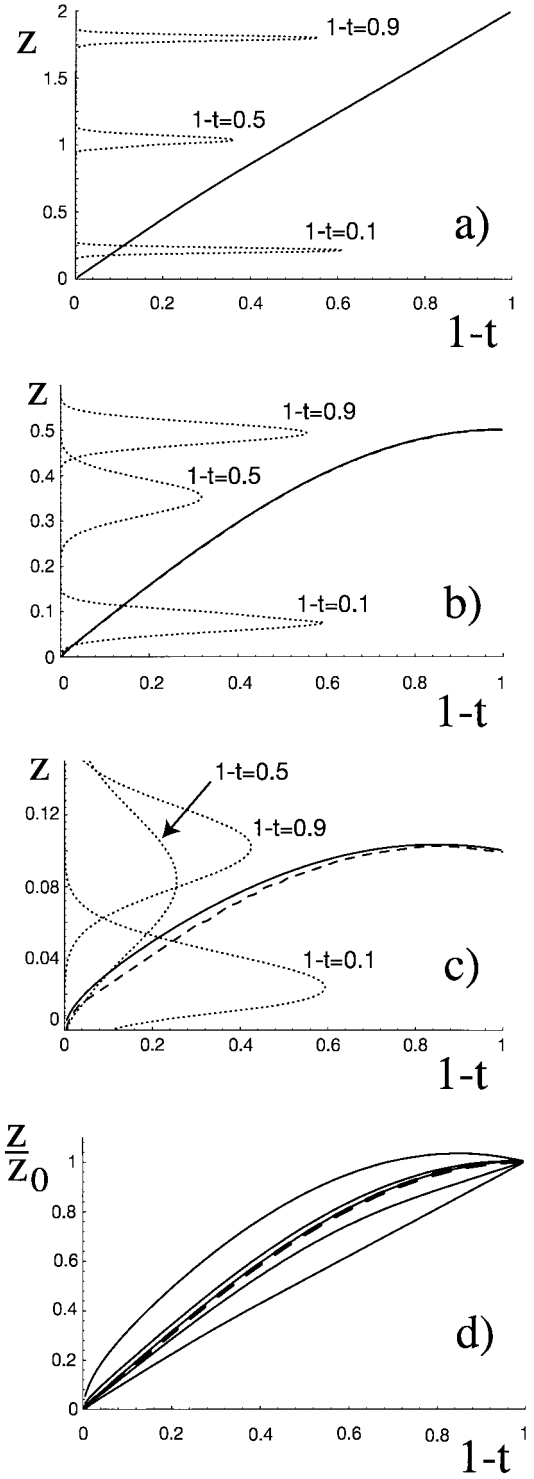

Figure 2. Scf results for $\beta = 100$, showing the average paths (solid curves) and the most probable paths (broken curves) for constrained end points at (a) $z_0 = 2$, (b) $z_0 = 0.5$, and (c) $z_0 = 0.1$. Also shown are the probability distributions for the monomer segments with $t = 0.1$, 0.5, and 0.9 (dotted lines). (d) Plot of the average paths rescaled by the end-point position for $z_0 = 2$, 1, 0.5, 0.24, and 0.1 (from bottom to top). The universal path of the infinite-stretching limit (ISL) is shown as a thick dashed line.

Our results for the statistics of end-constrained paths as a function of the amount of stretching in the brush and of the location of the end point are shown in the next three figures. The value of β is equal to 100, 10, and 1, in Figures 2−4, respectively. In parts a, b, and c of these figures, we plot the most probable paths

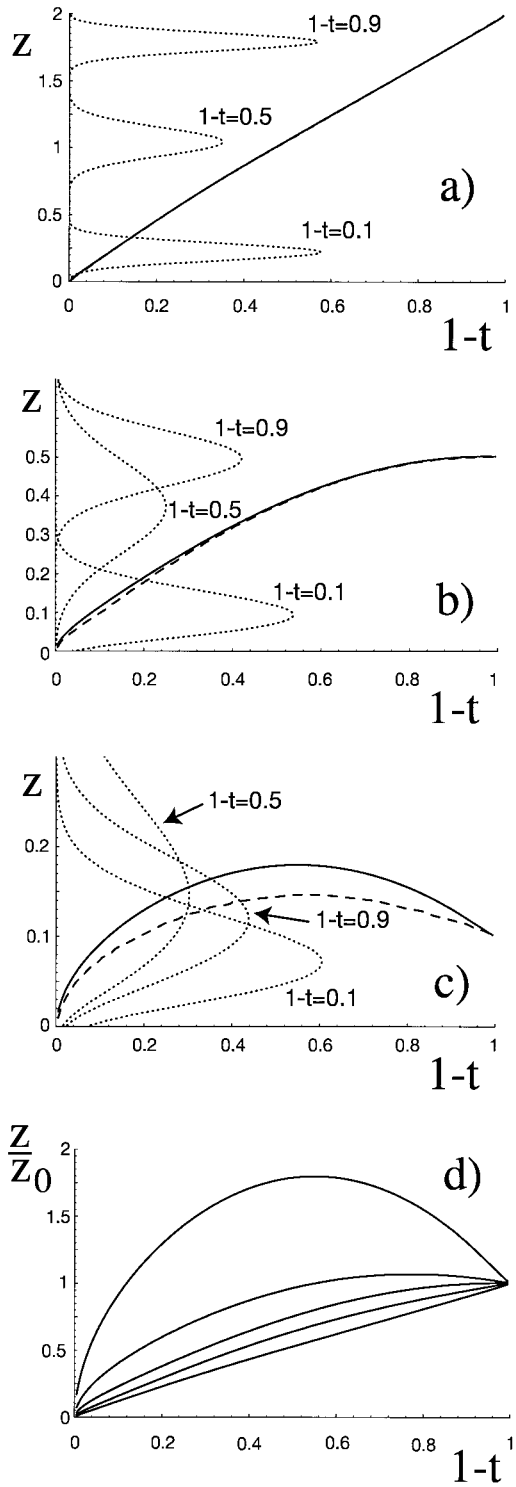

Figure 3. Scf results for polymer paths for $\beta = 10$, with the same notations as in Figure 2.

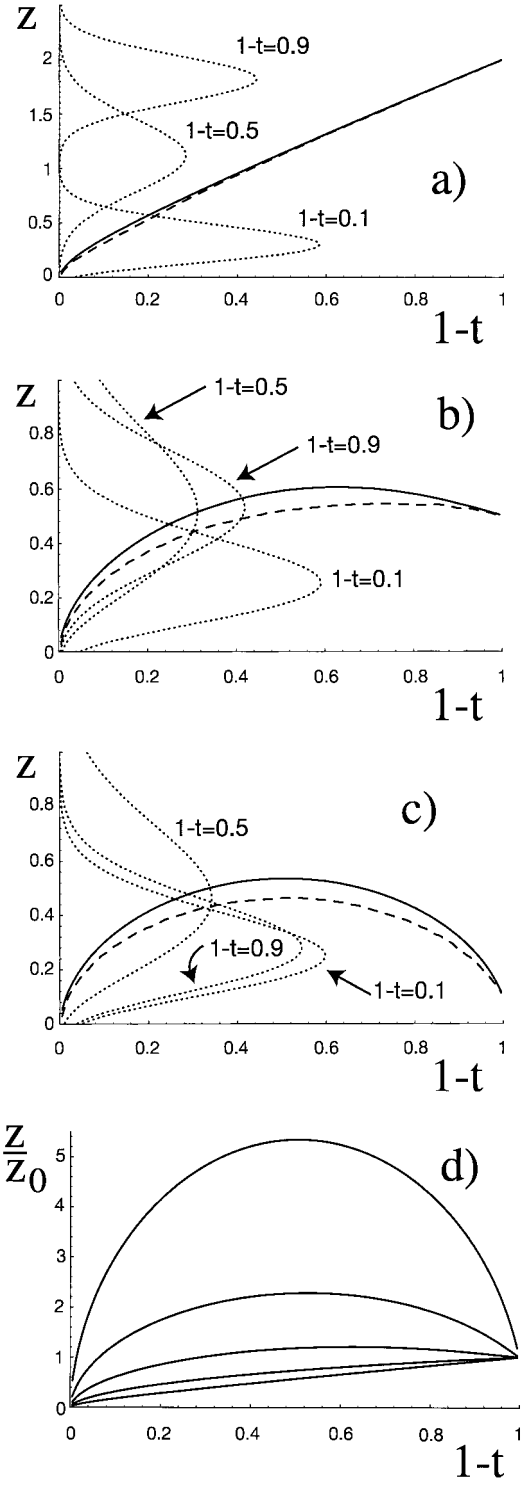

Figure 4. Scf results for polymer paths for $\beta = 1$, with the same notations as in Figures 2 and 3.

(dashed lines) and the average paths $\langle z(t)|_{z_0}\rangle$ (solid lines) of polymers whose end points are constrained to $z_0 = 2$, $z_0 = 0.5$, and $z_0 = 0.1$ respectively. The position is plotted as a function of the contour variable $1 - t$, so that the grafting surface is to the left, at $1 - t = 0$, and the free end is at the right, $1 - t = 1$. The dotted lines show the probability distribution $P(z,t)|_{z_0}$ itself for three values of the internal polymer coordinate; $1 - t = 0.9$, near the free end, $1 - t = 0.5$, and $1 - t = 0.1$, near the grafted end. In part d of the figures, we show the average paths rescaled by the end-point positions, $\langle z(t)|_{z_0}\rangle/z_0$, for end points constrained to $z_0 = 2$, 1, 0.5, 0.24, and 0.1 (from bottom to top).

We make three general observations, valid for all values of β. First, paths which start far from the grafting surface are stretched toward the wall through their entire length, including the free end point. The path shown which starts fartherest from the wall, $z_0 = 2$, is almost uniformly stretched, and appears as a straight line in Figures 2a, 3a, and 4a. The probability distributions of such polymers are rather narrow, and the average and most probable paths are almost indistinguishable (see Figures 2a, 3a, and 4a). Second, paths

which start close to the grafting surface are nonmonotonic, first moving away from the wall, reaching a maximum, and then turning toward the grafting surface (see Figures 2c, 3c, and 4c). Except at the maximum, all paths are stretched everywhere, including the end point. There is only one end-point position for which the paths are not stretched there. It follows that polymer paths which begin at different starting points are different in *form* as seen in Figures 2d, 3d, and 4d.

These results for the typical polymer paths are rather surprising, and seem to contradict scf results[25] which appear to show that the polymer paths are unstretched at the free end, in apparent agreement with the ISL theory of Milner, Witten, and Cates and of Zhulina et al. However we believe that in ref 25, all polymer paths were averaged over, regardless of their starting-point position z_0. As can be seen from Figures 2d, 3d, and 4d, the stretching, proportional to $dz/d(1-t)$, is positive for some of the most probable paths and negative for others, so that the average can be rather small even though it is not small for a most probable path beginning at some arbitrary starting point. This qualitative observations is further corroborated by results obtained within the classical theory; see section V.

As we increase the degree of stretching of the brush, as measured by the parameter β, the probability distributions for paths starting not too close to the wall become narrowly peaked, and average and most-probable paths move very close together (see Figures 2a, 2b, 3a). For the largest values of β, most of the polymers in the brush are strongly stretched, in the sense that most paths stay very close to the most probable, or classical, path. In Figure 2d we show the universal path obtained in the ISL as a thick dashed line. It is simply $z = \sin[\pi(1-t)/2]$. The actual paths are close to this form for an intermediate range of starting positions, but it is clear that there are distinct deviations for very small and very large end point positions. We will argue in a later section that these deviations are always present, even for extremely large values of β. That is, polymers which start far from the grafting surface are in general stretched throughout their length, including their end-points. They reach the limit of uniform stretching for end points sufficiently far from the surface. Polymers which start sufficiently close to the surface initially move away from it and reach a maximum before returning to it.

The physics behind these salient features is simple.

(1) A polymer which starts far beyond the bulk of the polymer brush is extremely stretched, and conformational fluctuations around the most probable path are strongly suppressed. Compared to the stretching contribution to the free energy, the interaction part is negligibly small. The stretching free energy is clearly minimized by a uniform stretching throughout the entire length. The fraction of polymers which do have free end points well beyond the bulk brush height decreases as β increases.

(2) A polymer which starts very close to the grafting surface is stretched little. Depending on the value of β, the repulsion between polymers or fluctuations around the classical path are dominant. For large values of β, excursions from the most probable path are costly, but the most probable paths of polymers which begin close to the wall initially move away from it because the decaying density profile exerts a force on the polymer segments which is directed away from the grafting surface. This argument explains the nonmonotonic path seen in Figure 2c which begins at $z_0 = 0.1$ in the strongly-stretched brush $\beta = 100$. For small values of β, fluctuations around the most probable path become important. In this case it is the entropic repulsion exerted by the impenetrable wall which is responsible for the nonmonotonic paths, and not the interactions between polymers. It is this effect which explains the nonmonotonic paths shown in Figures 3c and 4c which also begin at $z_0 = 0.1$, but for a moderately stretched brush, $\beta = 10$ and 1. We have verified these arguments by comparing the paths obtained in the scf of the interacting system with those obtained from the classical theory, which ignores excursions about the most probable path, and those obtained in a system in which the polymers only interact with the hard wall, but not with one another. Calculation of such paths is performed in section VI.

As is clear from these results, fluctuations around the classical paths are always unimportant if one considers paths which start sufficiently far away from the grafting surface. In particular a classical theory, which considers only a single path per starting point, should always be good at the outer perimeter of a brush and should describe most of the brush rather well, provided β is not too small. Such a classical theory should also be able to distinguish between the different paths taken by polymers which start far from the grafting surface and those which start close to it. These expectation are indeed borne out by our classical theory, advanced in the following section.

V. The Classical Approximation

Although the single particle partition function can be calculated numerically with relative ease, as we have shown in the last section, it is of interest to determine the classical approximation which retains only the most probable polymer configurations. To make this approximation clear, we first rewrite the single-polymer partition function within scf, $Q[\phi]$ of eq 18, by introducing end-constrained polymer paths $z(t,z_0) \equiv z(t)|_{z_0=z_0}$. The partition function becomes

$$Q = \int_0^\infty dz_0 \int_0^\infty Dz(\cdot,z_0) \exp\{-\beta \int_0^1 dt\, [\dot{z}^2(t,z_0) + \phi[z(t,z_0)]]\} \quad (29)$$

The classical approximation consists of replacing the functional integral over all polymer paths with constrained starting points z_0 by the integrand evaluated with the paths which minimize the mean-field free energy. This eliminates all but the most probable path for a given z_0. Thus

$$Q_{cl} = \int_0^\infty dz_0 \exp\{-\beta \int_0^1 dt\, [\dot{z}_{cl}{}^2(t,z_0) + \phi_{cl}[z_{cl}(t,z_0)]]\} \quad (30)$$

where the classical paths $z_{cl}(t,z_0)$ have to be determined by minimizing the system free energy. To restate: in the classical approximation, there is only a single path for a given starting point which contributes to the free energy. To determine this path, it is useful to interchange the dependent and independent variables describing the polymer path from $z_{cl}(t,z_0)$, with $z_{cl}(0,z_0) = z_0$ and $z_{cl}(1,z_0) = 0$, to $t(z,z_0)$, with $t(z_0,z_0) = 0$ and $t(0,z_0) = 1$. We also define the local stretching at z of a polymer which begins at z_0; $e(z,z_0) = -[dt\,(z,z_0)/dz]^{-1}$. Anticipat-

ing that paths which start at a z_0 very near the grafting surface may first move away from the surface before returning to it, as suggested by our scf results in the previous section, we define $z_m(z_0)$ to be the largest value of z attained by a path which begins at z_0. The single particle partition function in the classical approximation can then be written

$$Q_{cl} = \int_0^\infty dz_0 \exp\left\{-\beta \int_0^{z_m(z_0)} dz \left[\left|e(z,z_0)\right| + \frac{\phi_{cl}(z)}{|e(z,z_0)|}\right]\gamma(z,z_0)\right\} \quad (31)$$

For a polymer which first moves away from the wall and then turns around and approaches it, the path has two branches for distances $z_0 < z < z_m(z_0)$ and thus contributes twice to all integrals. This is accounted for by the function $\gamma(z,z_0)$, which is equal to unity for $z < z_0$ and to 2 otherwise, The self-consistent equation for the density follows from functional differentiation according to eq 20. In this classical limit, the equation becomes

$$\phi_{cl}(z) = \frac{1}{Q_{cl}} \int_{z_0(z)}^\infty \frac{\gamma(z,z_0)\, dz_0}{|e(z,z_0)|} \times \exp\left\{-\beta \int_0^{z_m(z_0)} dz' \left[\left|e(z',z_0)\right| + \frac{\phi_{cl}(z')}{|e(z',z_0)|}\right]\gamma(z,z_0)\right\} \quad (32)$$

where $z_0(z_m)$ is the inverse of $z_m(z_0)$. By comparing this equation with the constitutive relationship between the end-point distribution $g_{cl}(z_0)$ and the density

$$\phi_{cl}(z) = \int_{z_0(z)}^\infty dz_0 \frac{\gamma(z,z_0) g_{cl}(z_0)}{|e(z,z_0)|} \quad (33)$$

we find the end-point distribution to be

$$g_{cl}(z_0) = \frac{1}{Q_{cl}} \exp\left\{-\beta \int_0^{z_m(z_0)} dz \left[\left|e(z,z_0)\right| + \frac{\phi_{cl}(z)}{|e(z,z_0)|}\right]\gamma(z,z_0)\right\} \quad (34)$$

It follows from eq 31 that the end-point distribution is normalized to unity, i.e.

$$\int_0^\infty dz_0\, g_{cl}(z_0) = 1 \quad (35)$$

From eq 34, one obtains a simple expression for $-\ln Q_{cl}$, a quantity which is, of course, independent of z_0

$$-\ln Q_{cl} = \beta \int_0^{z_m(z_0)} \left[\left|e(z,z_0)\right| + \frac{\phi_{cl}(z)}{|e(z,z_0)|}\right]\gamma(z,z_0)\, dz + \ln[g_{cl}(z_0)] \quad (36)$$

This expression is made particularly transparent by multiplying it by $g_{cl}(z_0)$, integrating over all z_0, and using the normalization of $g_{cl}(z_0)$, eq 35, so that one obtains

$$-\ln Q_{cl} = \beta \int_0^\infty dz_0\, g_{cl}(z_0) \int_0^{z_m(z_0)} \left[\left|e(z,z_0)\right| + \frac{\phi_{cl}(z)}{|e(z,z_0)|}\right]\gamma(z,z_0)\, dz + \int_0^\infty dz_0\, g_{cl}(z_0) \ln[g_{cl}(z_0)] \quad (37)$$

Finally, substituting this into eq 21, we obtain the desired expression for the free energy of the many-polymer system in the classical limit

$$F_{cl} = -\frac{\beta}{2}\int_0^\infty dz\, \phi_{cl}^2(z) + \beta \int_0^\infty dz_0\, g_{cl}(z_0) \int_0^{z_m(z_0)} \left[\left|e(z,z_0)\right| + \frac{\phi_{cl}(z)}{|e(z,z_0)|}\right]\gamma(z,z_0)\, dz + \int_0^\infty dz_0\, g_{cl}(z_0) \ln[g_{cl}(z_0)] \quad (38)$$

The last term in the free energy is easily recognized to be the entropy associated with the end-point distribution. Just such a term was introduced in the context of the adsorption dynamics of brushes[28] and for copolymer melts,[29] but without the derivation which is provided here. Note that this entropy term is of order β^{-1} compared to the energy terms and is therefore absent in the infinite stretching, or $\beta^{-1} \to 0$, limit of the ISL theory of Milner, Witten, Cates, and Zhulina et al. As we show below, the presence of this term leads to qualitatively different results, even when β is large. The classical free-energy now has to be minimized subject to the following constraints.

(i) All polymers have equal length, i.e., in our rescaled units

$$\int_0^{z_m(z_0)} \frac{\gamma(z,z_0)\, dz}{|e(z,z_0)|} = 1 \quad (39)$$

(ii) The end-point density $g_{cl}(z_0)$ is normalized to unity, eq 35.

(iii) The monomer density $\phi_{cl}(z)$ is normalized to unity, eq 15.

(iv) The monomer density $\phi_{cl}(z)$ and end-point distribution $g_{cl}(z_0)$ satisfy the relation eq 33.

The last constraint is satisfied by the free energy (eq 38) at its minimum, as can be checked by variation of eq 38 with respect to $\phi_{cl}(z)$. Constraint iii is satisfied if constraints i and ii hold, as follows by integration of eq 33. The first two constraints are enforced by the usual method of undetermined Lagrange multipliers, i.e., by adding the terms

$$\int_0^\infty dz_0\, \Pi(z_0)\left[\int_0^{z_m(z_0)} \frac{\gamma(z,z_0)\, dz}{|e(z,z_0)|} - 1\right] + \lambda\left[\int_0^\infty g_{cl}(z_0) dz_0 - 1\right] \quad (40)$$

to the free energy. Variation with respect to the end-point distribution then leads to eq 34 (and thus satisfies the normalization eq 35) if the Lagrange multiplier λ is chosen as $\lambda = \ln Q - 1$. Variation with respect to $e(z,z_0)$ yields

$$e^2(z,z_0) = \phi_{cl}(z) - \phi_{cl}(z_0) + \pi^2(z_0) \quad (41)$$

where $\pi^2(z_0) \equiv \phi_{cl}(z_0) - \Pi(z_0)/\beta g_{cl}(z_0)$. The physical meaning of the Lagrange multiplier $\pi(z_0)$ is the mag-

nitude of the stretching of the polymer at its free end point positioned at z_0.

As noted by Johner and Joanny,[28] the end-point stretching $\pi(z_0)$ is related to the logarithmic derivative of the end-point distribution

$$\pi(z_0) = -\frac{1}{2\beta}\frac{\mathrm{d}\ln g_{\mathrm{cl}}(z_0)}{\mathrm{d}z_0} \tag{42}$$

It follows trivially that the sum of the end-point stretchings of all polymers is related to the probability of finding a polymer with its free end point at the grafting surface

$$\int_0^\infty \mathrm{d}z_0\, g_{\mathrm{cl}}(z_0)\pi(z_0) = \frac{1}{2\beta}[g_{\mathrm{cl}}(0) - g_{\mathrm{cl}}(\infty)] = \frac{g_{\mathrm{cl}}(0)}{2\beta} \tag{43}$$

From eq 42 it follows that classical paths starting close to the grafting surface, where the logarithmic derivative of $g_{\mathrm{cl}}(z_0)$ is positive, are expected to move initially away from the grafting surface. They must ultimately turn back and approach the wall. Classical paths starting further away from the grafting surface, where the end-point distribution decreases, are predicted to move monotonically toward the wall. The integral over the end-point stretching of all polymers, eq 43, is expected to be very small due to the factor of β in the denominator. Although strictly derived only for the classical limit, this result is in accord with the result of Milner,[25] who found the average end-point stretching in his scf results to be negligible. In the limit in which $\beta \to \infty$, eq 42 shows that the end-point stretching vanishes, in agreement with the ISL theory. In the same limit the entropy term associated with the end-point distribution in eq 38 can be neglected, and as we will demonstrate in Appendix A, the free energy is minimized by the asymptotic classical solution of the ISL theory given in refs 5 and 6.

At finite β, however, the results are markedly different as can be seen from Figure 5a where density profiles $\phi_{\mathrm{cl}}(z)$ for four different values of β are plotted. They show an exponential tail and, as β decreases, deviate substantially from the ISL parabolic solution (shown as a thick dashed line). Figure 5b shows the corresponding end-point distributions $g_{\mathrm{cl}}(z_0)$, which again deviate substantially from the ISL result (shown as a thick dashed line) as β decreases (the data are replotted on an extended scale in Figure 7). The entropic term forces g_{cl} to be nonzero everywhere for finite β. As this parameter decreases, the entropy of the end-point distribution becomes increasingly important. Because this effect is ignored by scaling arguments, the estimate of the brush height given by such arguments becomes poorer. Thus, while β is still the square of the ratio of the brush height as given by scaling arguments to the radius of gyration, it can no longer be interpreted as the ratio of the square of the *actual* brush height to the radius of gyration.

The classical paths are, in general, stretched everywhere, including their free end point, in agreement with the path analysis within the scf theory. Figure 5c shows, for four values of β, the function $e(z_0,z_0)$ whose magnitude is the stretching at the end point. Not surprisingly, those few paths which start far from the surface are greatly stretched there, and the value of $e(z_0,z_0)$ approaches a straight line with a slope of unity (heavy broken line), which represents a uniformly stretched path. The negative value of e for paths which start close to the surface indicates that these paths

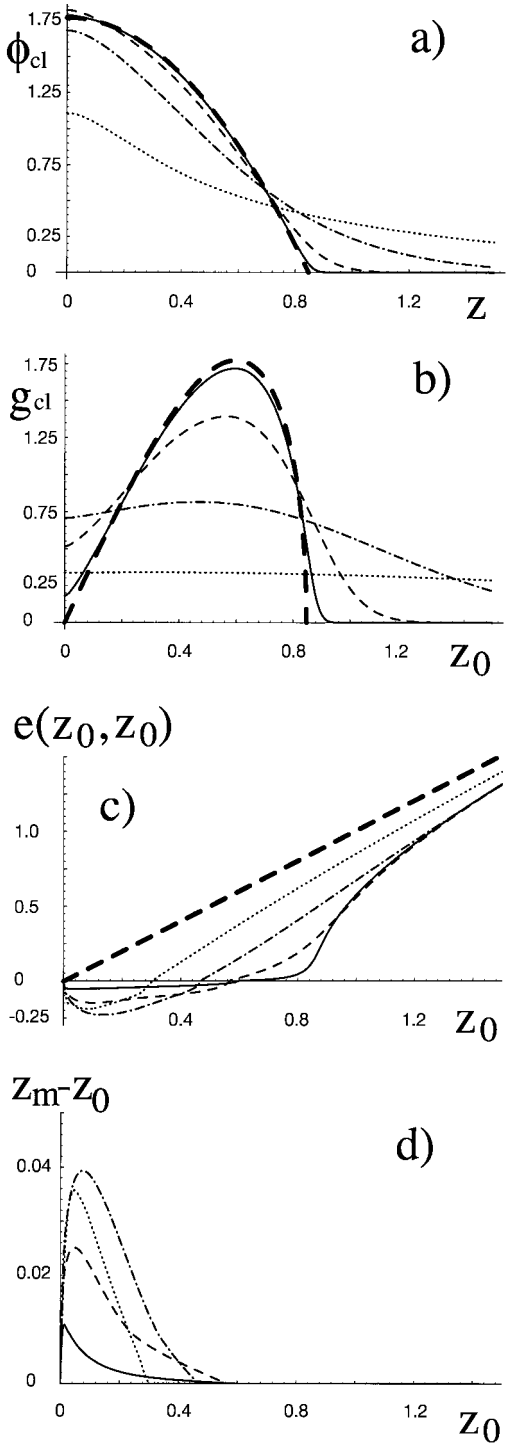

Figure 5. (a) Classical results for the rescaled density profiles ϕ as a function of the rescaled distance z from the grafting surface. Shown are results for $\beta = 0.1$, 1, 10, and 100 (dotted, dash−dotted, dashed, and solid lines, respectively), progressively approaching the asymptotic result (valid for $\beta \to \infty$), shown as a thick dashed line. (b) Rescaled end-point distribution g as a function of the end-point position z_0. The results are for the same values of β as in part a and again approach the asymptotic result (thick dashed line). (c) End-point stretching $e(z_0,z_0)$ as a function of the end-point position z_0, for the same parameters as in part a. Negative values indicate that the path moves away from the grafting surface. The heavy broken line is of slope unity and denotes the expected end-point stretching for uniform stretching. (d) Difference between maximum z_m (z_0) and end-point positions z_0 for the same parameters as in part a.

initially move away from the surface before turning back, in agreement with our self-consistent results. Figure 5d shows the difference between the maximum value z_m which these paths attain and their end-point value. Interestingly, this difference first increases with decreasing values of β, but the curve for $\beta = 100$ (dotted curve) lies entirely below the curve for $\beta = 10$ (dashed-dotted curve).

For large β the results of our classical theory approach those of the ISL theory of Milner, Witten, Cates, and Zhulina et al., which is demonstrated in Appendix A. There we also calculate the free energy within the ISL theory. As expected, the free energy of our classical theory is always lower than the free energy of the ISL solution corresponding to the parabolic brush profile.

VI. Comparison between Self-Consistent Field Theory and Classical Theory

As argued in the previous sections, the strong stretching of polymers almost everywhere for moderately large values of β, and at the perimeter of the brush for almost all values of β, makes the classical approximation a reasonable one. Just how accurate it is can be tested by comparison to the self-consistent results.

In parts a−d of Figure 6, we plot the density as obtained from our classical theory (solid line) and the self-consistent density (dashed line) for four values of β: 100, 10, 1, and 0.1, respectively. For the largest value of β, Figure 6a, the two densities are virtually indistinguishable except for the immediate vicinity of the wall, where the self-consistent density drops. For smaller values of β this density decrease near the wall becomes more pronounced. The *form* of the decrease in the tail of the scf density profile is reproduced extremely well by the classical theory. This is obscured in a direct comparison of the two profiles because they have the same normalization, yet the profile of the scf, shown as a dashed line, which feels the entropic repulsion of the grafting surface, is displaced from that surface, while the classical result, shown as a solid line, is not. To verify that the forms of the density profile in the tail are indeed the same, we show with a dotted line the scf profile simply displaced toward the wall until the tails of the scf and classical distributions coincide. The size of the displacement needed to bring about this coincidence depends on β.

In parts a−d of Figure 7, we plot the end-point distribution calculated within our classical approximation (solid line) and the self-consistent method (dashed line). Again, for $\beta = 100$, Figure 7a, the two curves are very similar, except for the behavior near the wall. This difference increases as β decreases, but again the form of the decay of the end point distribution, $g(z_0)$, with the end point location, z_0, is captured very well by the classical theory. This is again shown by simply shifting the self-consistent results toward the wall, the result of which is shown by a dotted line.

The asymptotic behavior of the end-point distribution and the density for larger distances will be discussed in section VI.B.

A. Comparison of Individual Polymer Paths. As we have emphasized, in the classical approximation, only one path which originates at a given end point is considered, and it is obtained by minimizing the free energy contributed by the distribution of such paths. In the full scf, all possible paths are considered. A different approximation consists in neglecting the interaction between polymers altogether, which is valid for the entire brush in the limit $\beta \to 0$ and for all values of β for the outer perimeter of the brush. We use this approximation, which is introduced in Appendix B, mainly to discuss the effects of the impenetrable grafting wall and to show that some of the effects found in the self-consistent and classical theory, mainly the stretched end-points and the nonmonotonic paths, are already present in this limit. One way of assessing the importance of the fluctuations about the classical paths is to compare the most probable path for a given end point as obtained from the full scf with the classical path having the same end point. We make that comparison in this section for four paths with different end points,

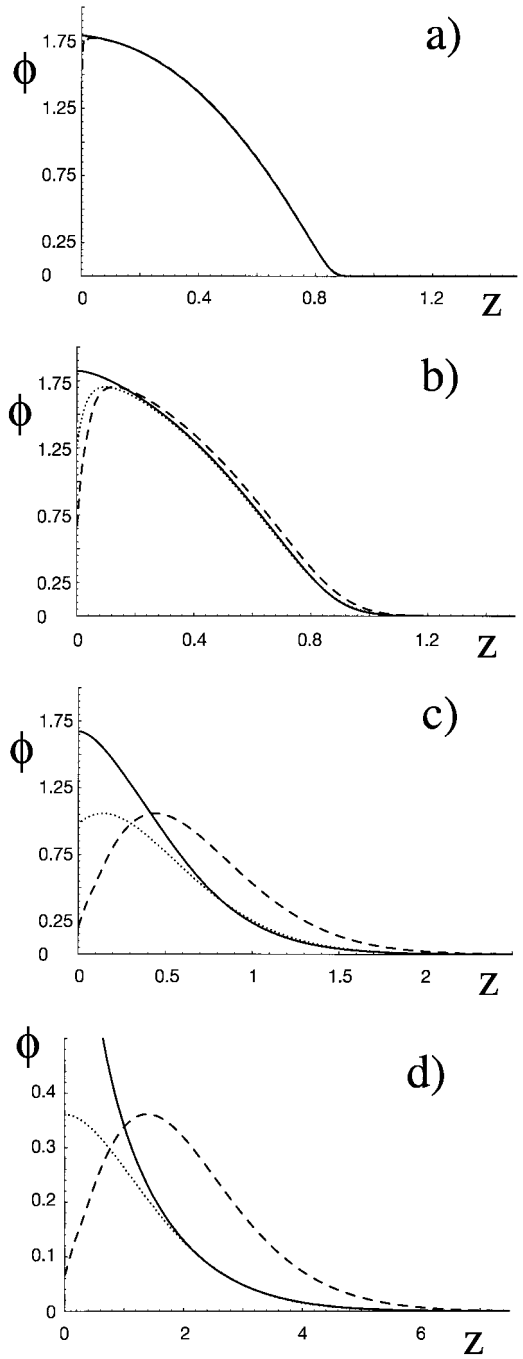

Figure 6. Comparison of the monomer density $\phi(z)$ obtained with scf theory (broken line) and the classical theory (solid line) for (a) $\beta = 100$, (b) $\beta = 10$, (c) $\beta = 1$, and (d) $\beta = 0.1$. The dotted line denotes the scf theory results shifted to the left by an amount which depends on β.

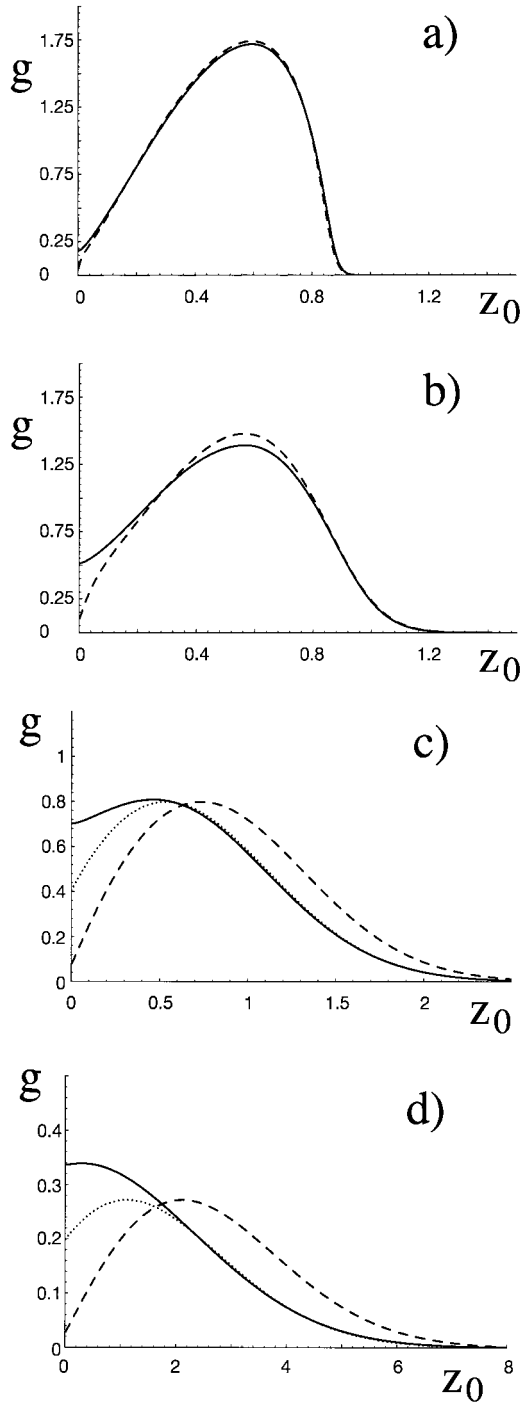

Figure 7. Comparison of the end-point distribution $g(z_0)$ obtained with scf theory (broken line) and the classical theory (solid line) for (a) $\beta = 100$, (b) $\beta = 10$, (c) $\beta = 1$, and (d) $\beta = 0.1$. The dotted line denotes the scf theory results shifted to the left by a variable amount.

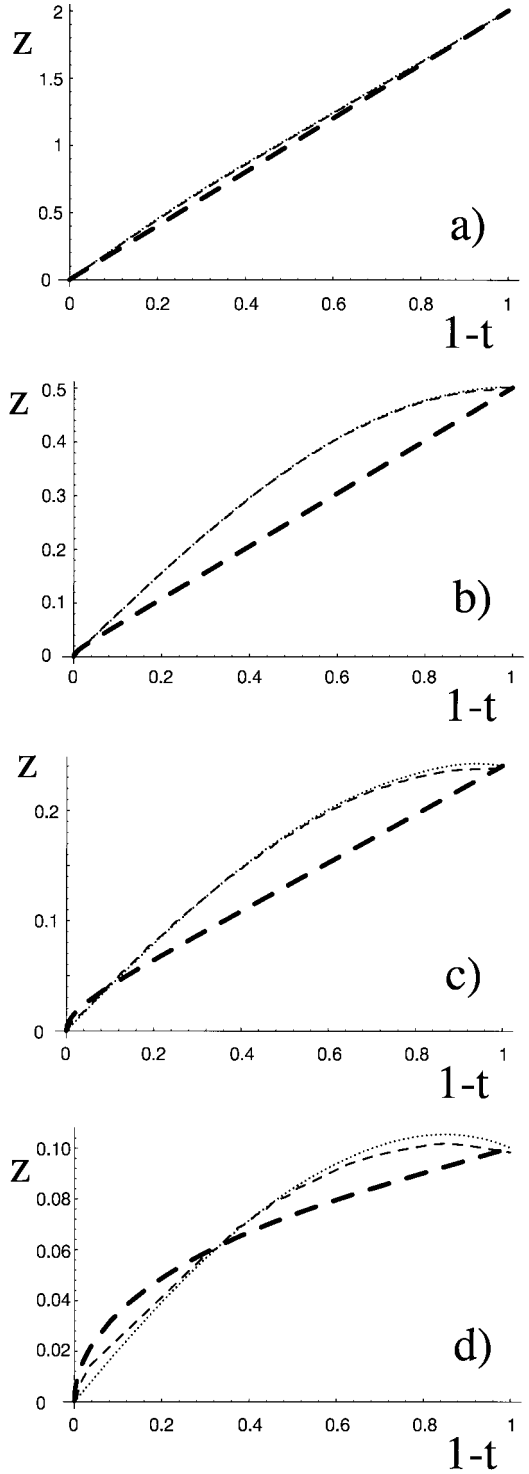

Figure 8. Comparison of scf and classical theory results for polymer paths for $\beta = 100$ and end-points constrained to (a) $z_0 = 2$, (b) $z_0 = 0.5$, (c) $z_0 = 0.24$, and (d) $z_0 = 0.1$. The scf results for the most probable paths are denoted by broken lines, while the paths obtained within the classical theory are denoted by a dotted line. The heavy broken lines give the predictions of the exactly solvable interaction-free theory.

z_0, embedded in brushes with three different degrees of stretching, β. Figure 8 shows paths in a strongly stretched brush, $\beta = 100$, one in which we expect the classical theory to be good. Figure 8a shows a path which begins at $z_0 = 2$, well outside the bulk of the brush, which, as seen in Figure 6a, extends to about $z = 0.85$. The most probable path as calculated from the full scf is shown with a broken line, and that from the classical theory is shown as a dotted line. They are almost indistinguishable and represent a path which is uniformly stretched. This becomes more evident by comparison with the average path calculated within the interaction-free theory, which is denoted by a heavy broken line. Parts b and c of Figure 8 show that for a path that begins well inside the brush, at $z_0 = 0.5$ and $z_0 = 0.24$, the classical and scf paths are still very similar. There are pronounced differences from the path of the noninteracting theory, which means that the repulsive interaction between monomers is the driving force for the path characteristics within both the scf

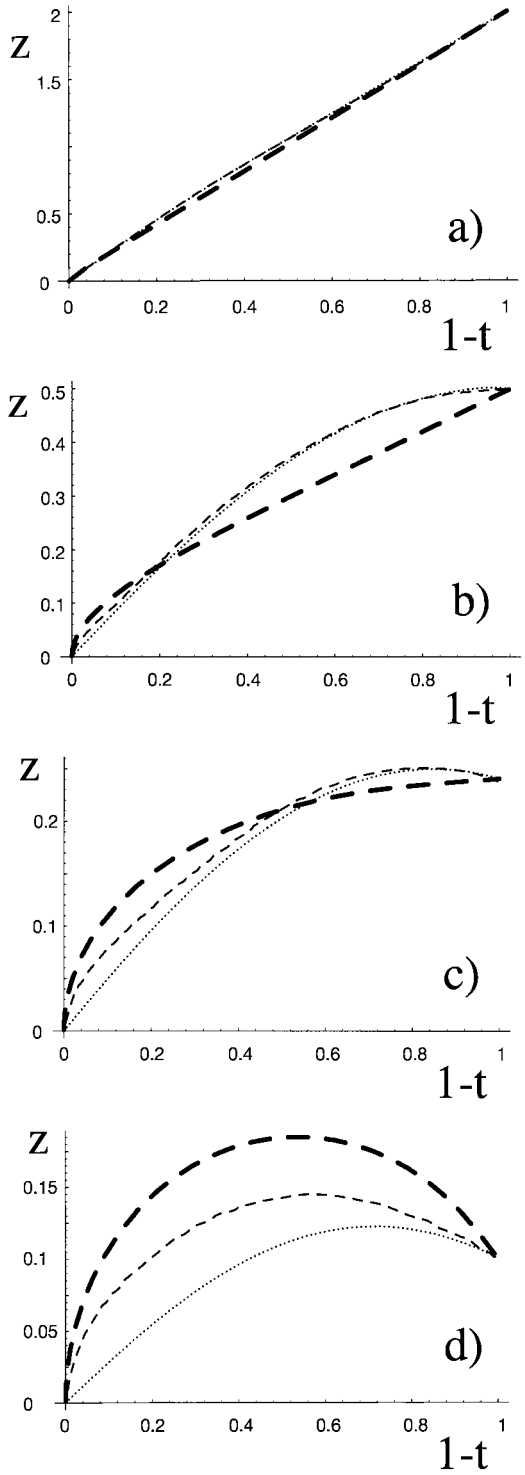

Figure 9. Comparison of scf and classical theory results for polymer paths for $\beta = 10$ with the same parameters and notations as in Figure 8.

theory and the classical theory. For a path which begins very close to the wall, $z_0 = 0.1$, Figure 8d shows that there is some small difference between the classical and scf paths. Both paths move away from the wall initially before returning to it. At this value of β, this effect is due entirely to the interactions, that is, to the fact that the decreasing density profile causes a force on the polymer directed away from the wall. This is evident because the path of the non-interacting theory is monotonic.

Parts a−d of Figure 9 show the same sequence for a brush much less strongly stretched, $\beta = 10$. The density profile of this brush, shown in Figure 6b, still does not extend much beyond z of about 0.9. Thus a path which begins at $z_0 = 2$, as in Figure 9a, is still uniformly stretched and very well described by the classical theory. Both the classical and the scf paths are very similar to the noninteracting path (heavy broken curve). The classical description is also very good for the path which begins well within the brush at $z_0 = 0.5$, as can be seen from Figure 9b. In parts c and d of Figure 9, the paths of the classical approximation are quite distinct from the most probable paths within the full scf, although the nonmonotonic nature of the paths is captured. The difference in the classical and scf paths for $z_0 = 0.1$, Figure 9d, reflects the fact that, at this value of β, the nonmonotonic nature of paths starting very close to the wall is mostly due to the entropic repulsion of the wall, which the scf calculation feels but which the classical approximation does not. This is evident from comparison with the path of the noninteracting theory (bold broken line), which shows an even stronger nonmonotonic behavior than the scf path; see Figure 9d. In this case, the interaction actually pushes the monomes *closer* to the wall because the monomer density initially increases as one moves away from the wall.

Finally, in Figure 10, we compare paths in a brush which is hardly stretched at all, $\beta = 1$. The profile of this brush is shown in Figure 6c. A polymer which is stretched beyond the bulk of the brush is still well described by our classical theory, as seen in Figure 10a. The difference between the scf and classical theories is now greater for paths beginning within the brush at $z_0 = 0.5$, and even more so for those beginning very near the wall at $z_0 = 0.24$ or $z_0 = 0.1$. Again this is due to the increased importance of the entropic repulsion of the wall in a weakly stretched brush. Thus we see that differences between our classical and the scf theory become more pronounced as β decreases and become observable for progressively larger end-point positions. However the qualitative features of the path statistics as determined by the self-consistent treatment of the interacting system are captured well by the classical approximation, even for values of β as small as unity. These features are the near-uniform stretching of paths with large values of the end point, and the nonmonotonic behavior of paths with end points close to the grafting surface.

B. Behavior for Large Distances. ***1. Classical Theory.*** For large distances from the grafting surface the behavior simplifies enormously. As we saw in the self-consistent and classical results, paths with large values of the starting position are almost uniformly stretched, i.e. the stretching function e is given by

$$e(z,z_0) \simeq z_0 \tag{44}$$

independent of z. Using this approximation in the classical expression for the end-point distribution, eq 34, and employing the normalization of ϕ, eq 15, the end-point distribution can be written down immediately as[30]

$$g(z_0) \simeq \frac{1}{Q} \exp\{-\beta(z_0^2 + 1/z_0)\} \tag{45}$$

Thus plots of $\ln[g(z_0)]/\beta$ vs z_0 when shifted by a β-dependent constant should be the same for all β at large z_0. Figure 11a shows such a plot of the classical results for the end-point distribution for the four different

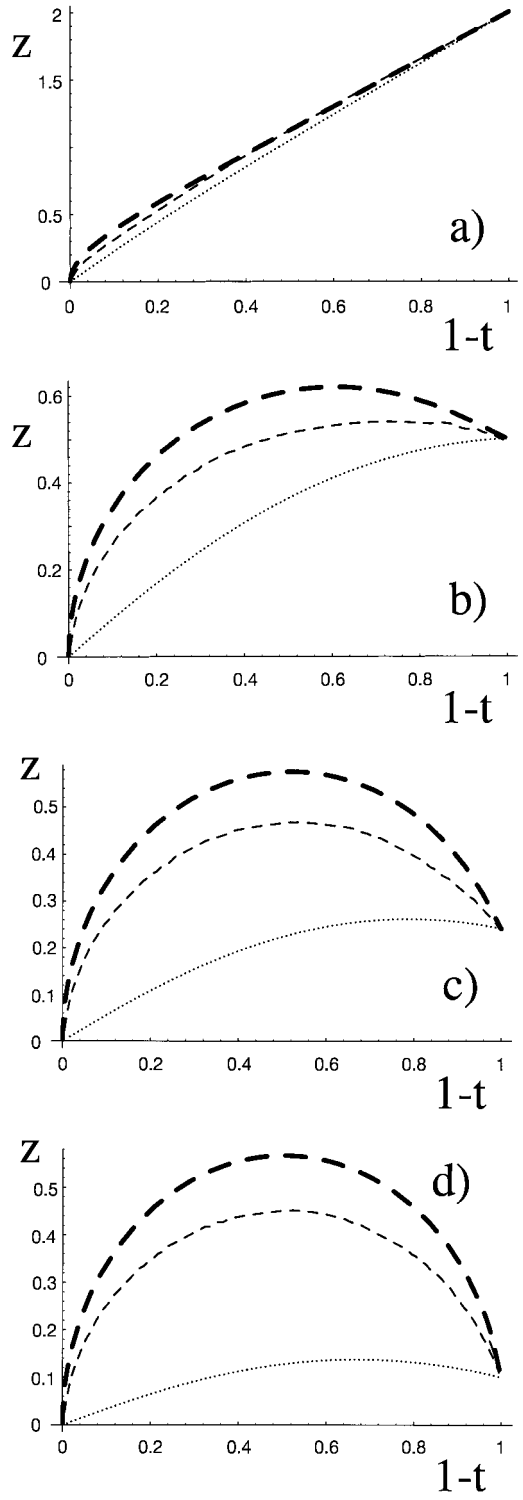

Figure 10. Comparison of scf and classical theory results for polymer paths for $\beta = 1$ with the same parameters and notations as in Figure 8 and 9.

values of β already shown in Figure 5b, together with the prediction eq 45 (dashed line). The β-dependent constant has been chosen so that all data coincide for $z_0 = 2$. The fit is excellent. We also show a purely Gaussian distribution

$$g(z_0) \sim \exp\{-\beta z_0^2\} \tag{46}$$

denoted by a solid line. As can be seen, the asymptotic scaling of eq 45 describes the data quite well for the larger values of z_0, which indicates that the effect of the interaction is negligible for polymers paths ending far away from the wall. The density can be readily calculated according to eq 33 if one neglects the interaction term inversely proportional to z_0 in the expression for the end-point distribution, eq 45. The result is

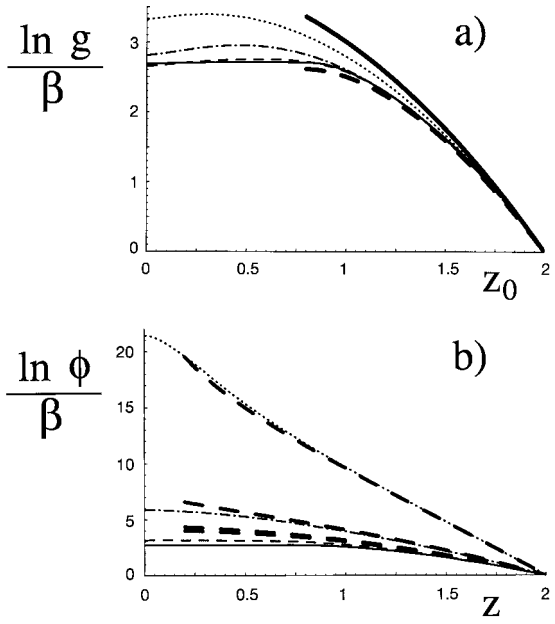

Figure 11. Asymptotic results of the classical theory. (a) Shown are the results for the end-point distribution for the same parameters as in Figure 5b plotted as $[\ln g(z_0)]/\beta$ plus a β-dependent constant. The prediction according to eq 45 is plotted as a heavy broken line. The heavy solid line denotes the behavior of a purely Gaussian end-point distribution, eq 46. (b) Shown are the results for the monomer density for the same parameters as in Figure 5a plotted as $[\ln \phi(z)]/\beta$ plus a β-dependent constant. The predictions according to eq 47 are plotted as heavy broken lines.

$$\phi(z) \simeq \mathrm{Ei}(-\beta z^2)/2 \tag{47}$$

where $\mathrm{Ei}(x)$ is the exponential integral. For large arguments, this approximation to the classical density behaves as

$$\phi(z) \sim \frac{\exp(-\beta z^2)}{2\beta z^2} \tag{48}$$

This again suggests plotting $\ln[\phi(z)]/\beta$ shifted by a β-dependent constant *vs.* z for several values of β. We do so in Figure 11b where we have chosen the β-dependent constants so that all curves coincide as $z = 2$. We also show the approximations according to eq 47 as heavy broken curves, shifted so that they pass through the same point. The agreement is quite satisfactory. According to eq 48, the density profile in the tail of the distribution is essentially Gaussian, $\phi \sim \exp(-\beta z^2) \sim \exp(-3r_\perp^2/2Na^2)$. This is just the distribution expected from ideal, noninteracting chains, and it arises because the interaction energy of chains whose end points are well beyond the average brush height is small compared to their stretching energy. Furthermore, the uniform stretching observed for such chains is also characteristic of ideal chains.

2. Self-Consistent Field Theory. The major difference between the self-consistent and classical theories arises from the fact that the former includes the entropic repulsion due to the wall while the latter does

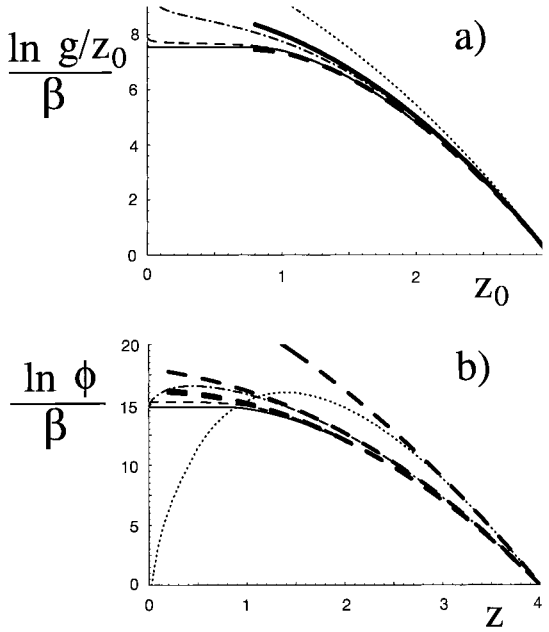

Figure 12. Asymptotic results of the scf theory. (a) Shown are the results for the end-point distribution for the same parameters as in Figure 1b plotted as $[\ln g(z_0)/z_0]/\beta$. The prediction according to eq 49 is plotted as a heavy solid line. The heavy broken line denotes the behavior of an approximation which takes the interactions into account; see text. (b) Shown are the results for the monomer density for the same parameters as in Figure 1a plotted as $[\ln \phi(z)]/\beta$. The predictions according to eq 50 are plotted as heavy broken lines.

not. The entropic repulsion of the wall is also accounted for in the noninteracting system, presented in Appendix B. Furthermore the interaction-free theory should provide a good approximation to scf results at large distances because for polymers with end points far from the wall, the stretching contribution to the free energy is much larger than that due to interactions.

The end-point distribution $g(z_0)$ of the free theory is, according to eqs 26 and B4, given by

$$g(z_0) \simeq 2\beta z_0 \exp(-\beta z_0^2) \tag{49}$$

The only difference between this and the asymptotic classical result, eq 46, is the prefactor of z_0, which reflects the entropic, repulsive pressure due to the wall. In Figure 12a we plot $\ln[g(z_0)/z_0]/\beta$ for the three different values of β shown already in Figure 1b, together with the approximation eq 49 (full line). We also show the behavior of the function $g(z_0) \simeq z_0 \exp[-\beta(z_0^2 + 1/z_0)]$, dashed line, which takes the interactions into account in an approximate fashion. All data are normalized so as to coincide for $z_0 = 3$. As can be seen, the asymptotic scaling of eq 49 describes the data quite well for the larger values of z_0. However for the larger values of β, i.e., for the solid line ($\beta = 100$) and the broken line ($\beta = 10$), the monomer−monomer repulsion is important for intermediate values of z_0, and here the approximation denoted by the broken line gives better agreement. The difference between the two heavy lines is small for large values of z_0.

An approximation for the density $\phi(z)$ at large z can be obtained from the end-point distribution of the free theory, eq 49, and the assumption of uniform stretching, eq 44. Using these approximations in the constitutive relation, eq 33, one obtains

$$\phi(z) \simeq \frac{1}{2}\sqrt{\frac{\pi}{\beta}}\,\mathrm{erfc}(\sqrt{\beta}z) \tag{50}$$

For large distances z, this result behaves as

$$\phi(z) \sim \frac{\exp(-\beta z^2)}{\beta z} \tag{51}$$

Once again, we see that the decay of the density is essentially Gaussian, just as in the classical theory, eq 48. In Figure 12b we replot the densities from Figure 1a as $\ln[\phi(z)]/\beta$, together with the approximation of eq 50, again scaled so that all data coincide as $z = 4$. The agreement is satisfactory. The asymptotic limit where the data are predicted to scale according to eq 51 is only reached for the two largest values of β.

This Gaussian decay contrasts with the $\phi \sim \exp[-(z - z_m)^{3/2}]$ prediction of ref 31 for the density profile in the immediate vicinity of the brush edge. This form was obtained by taking into account, in an approximate fashion, fluctuations around the classical paths of the infinite-stretching, $\beta \to \infty$, limit. We looked for a behavior $\sim\exp[-(z - z_m)^{3/2}]$ at intermediate length scales in our scf results but were not able to detect such a decay over any appreciable range of data. A different method was used in ref 32, where path fluctuations around a steplike density profile were taken into account, leading to a profile decaying asymptotically as $\phi \sim 1/\beta z^2$.

These different results show that care must be taken in the choice of the density profile around which one expands when considering the effect of fluctuations about the classical paths.

VII. Discussion

This paper contains the derivation and solution of the classical theory for polymer brushes, together with a detailed comparison with numerical results of a self-consistent field theory. Self-consistent field methods have been applied to polymer brushes before, but the fact that the continuum theory depends on a single parameter, β, which measures the degree of stretching, has not been used to its full potential. The classical theory reduces to the infinite-stretching theory of Zhulina et al. and Milner et al. in the limit $\beta \to \infty$, but is not a systematic expansion about this limit. It is simply the theory which results from ignoring the contribution to the free energy from all polymer paths other than the most probable ones. We find some results of the classical and the scf theory to be comparable even for values of β which are small. These include the properties of the brush at large distances from the wall. Such a result is easily understood because the properties at large distances are dominated by strongly stretched configurations. On the other hand, properties of the brush near the grafting surface itself are not captured well by the classical theory except for larger β, because it misses the entropic repulsion of the wall.

The conditions of applicability of the self-consistent field and classical theory presented in this article are obviously important. As discussed in section II the second virial expansion we employ breaks down close to the Θ point and at densities near close-packing, but we will not be concerned with the consequences here. The approximations we have made limit the applicability of the present results in two essential ways. The

first approximation is to ignore the correlations of density fluctuations, which is the signature of mean-field theory, and the second is to ignore all but the most probable polymer configurations, which is the classical approximation.

We discuss the validity of the mean-field approximation first. The weak requirement for mean-field theory to be applicable is that one chain interacts with many other chains. This condition is satisfied if the surface coverage is greater than that characteristic of the mushroom regime[33] based on the swelling behavior in good solvent. This condition requires

$$\sigma a^2 > N^{-6/5}\left(\frac{w}{a^3}\right)^{-2/5} \tag{52}$$

and tells us that the polymer chains become ideal at large length scales due to screening of the excluded volume interaction. We now want to derive the much stronger condition under which the polymer chains are ideal on *all* length scales. To that end we define the Gaussian blob size ξ_G, which is the size of a single polymer coil below which the excluded volume interaction w is irrelevant. The blob size ξ_G and the number of monomers in the Gaussian blob, N_G, are obviously related by $\xi_G \sim aN_G^{1/2}$. A simple Flory argument determines the crossover monomer number N_G to be

$$N_G \sim \left(\frac{w}{a^3}\right)^{-2} \tag{53}$$

For a much longer polymer with $N > N_G$ these Gaussian blobs act as noninterpenetrating subunits, so that the polymer size ξ is given by

$$\xi \sim \left(\frac{N}{N_G}\right)^{3/5}\xi_G \sim aN^{3/5}\left(\frac{w}{a^3}\right)^{1/5} \tag{54}$$

The polymers in a brush are strongly stretched and thus break up into stretching blobs of size ξ_S containing N_S monomers each.[34] Due to the effective force acting on these blobs they align in a row so that the brush height h is determined by

$$h \sim \frac{N}{N_S}\xi_S \tag{55}$$

which, using the scaling relation eq 54 for ξ_S, leads to a formula for the number of monomers inside a stretching blob in terms of the brush height

$$N_S \sim \left(\frac{aN}{h}\right)^{5/2}\left(\frac{w}{a^3}\right)^{1/2} \tag{56}$$

The monomer concentration inside a stretching blob can thus be written as

$$c_S \sim \frac{N_S}{\xi_S^3} \sim \frac{h^2}{wa^2N^2} \tag{57}$$

The average monomer concentration in a brush of height h is obviously given by $c \sim N\sigma/h$. Assuming a close packing of the stretching blobs, i.e., $c = c_S$, we infer the brush height to scale like $h \sim N(w\sigma a^2)^{1/3}$, in agreement with the original Flory prediction and our results. The polymers are ideal on all length scales if the number of monomers in a stretching blob is smaller than the number of monomers in a Gaussian blob, which means

$$\frac{N_S}{N_G} \sim \left(\frac{w^2}{\sigma a^8}\right)^{5/6} < 1 \tag{58}$$

Together with the constraint that the monomer area fraction on the grafting surface is smaller than unity, $\sigma a^2 < 1$, this leads to the following condition under which the mean-field approximation is valid:[5]

$$\left(\frac{w}{a^3}\right)^2 < \sigma a^2 < 1 \tag{59}$$

Which of the lower bounds on σa^2 is more restrictive, eq 52 or eq 59? The answer depends on the excluded volume interaction. If $(w/a^3)^2 > 1/N$, the lower bound eq 59 is more restrictive, since the chains need to interact with other chains in order to be ideal. If however $(w/a^3)^2 < 1/N$, the chains are ideal on all length scales even without being stretched; this corresponds to relatively short chains close to the Θ point, for which higher order virial coefficients are important and our model breaks down. It is therefore the bound eq 59 which limits the applicability of the mean-field approximation within the present context.

For the Gaussian chain model to be applicable, we need the brush height to be smaller than the contour length of the polymer, i.e., $h < Na$. Inserting the scaling result for h, we obtain $w/a^3 < 1/(\sigma a^2)$. Since the grafting area fraction σa^2 is smaller than unity, this condition is always fulfilled in the case where mean-field theory is valid, i.e., where condition eq 59 holds.

The discussion was based so far on uniform stretching and a uniform density within the brush. Assuming condition eq 59 to hold, we ask where in the brush should we expect the mean-field approximation to break down locally? This will occur only if the polymer stretching and the monomer concentration are both locally smaller than average, so that the stretching blobs can swell beyond the Gaussian blob size without reaching the close-packing limit of blobs. Repeating the above analysis for a spatially varying monomer density $\phi(z)$ and polymer stretching dz/dt, we find that the condition for a local break-down of the mean-field assumption is

$$\left\{\phi(z) \text{ and } \left(\frac{dz}{dt}\right)^2\right\} < \left(\frac{w^2}{\sigma a^8}\right)^{2/3} \tag{60}$$

Close to the grafting surface the density decreases, but the average stretching of polymers is nonzero. The scaling analysis therefore does not predict a breakdown of mean field theory here. At the perimeter of the brush, however, the average stretching of the polymers is small and the concentration decreases drastically, also. It is therefore in the small region between the maximum in the end-point distribution (where the end-points of the polymers tend to have low tension and the density is already lower than unity; see parts a and b of Figure 1) and a little further away from the grafting surface (where the polymers tend to be stretched rather uniformly, see Figures 2d, 3d, and 4d) that correlation effects might be important, depending on the value of the constant $w^2/\sigma a^8$. Contrary to what one might expect, correlation effects are negligible as one moves far away from the grafting surface. Although the density reaches zero exponentially, the chains are so strongly stretched

that the self-interaction is irrelevant (assuming that inequality eq 59 holds).

Validity of the classical approximation requires that the chains be strongly stretched on average, i.e., $\hat{z}^2/a^2N = 2\beta/3 > 1$. With the definition of β above, this leads to a lower bound on the excluded volume interaction, which can be written as

$$\frac{1}{\sigma^2 a^4 N^3} < \left(\frac{w}{a^3}\right)^2 \tag{61}$$

Combining this constraint with eq 59, one obtains a window of applicability for the grafting density, $1/N < \sigma a^2 < 1$, a window which is easy to satisfy experimentally. As can be seen from Figures 2d, 3d, and 4d the chains are not stretched equally, and we expect that the classical approximation will be poor near the wall where the stretching is small but will be excellent in the region of the tail where the stretching is large. These expectations are confirmed by comparison of our classical results with those of the full self-consistent theory even for values of β on the order of unity. Thus there is an ample region over which results of the classical theory should be valid, and it will be of interest to study its application to other polymer systems.

Acknowledgment. We acknowledge useful discussions with J.-F. Joanny, A. Johner, H. Orland, and C. Seidel. This work was supported in part by the National Science Foundation under Grant No. DMR9531161.

Note Added in Proof

The non-vanishing end point stretching of individual polymer paths has recently been confirmed using molecular dynamics simulations of grafted chains (C. Seidel and R. R. Netz, to be published).

Appendix A: The Infinite Stretching Limit, $\beta \to \infty$

For large β the results of our classical theory approach those of the ISL theory of Milner, Witten, and Cates and Zhulina et al. In this section we show that, indeed, our theory reduces to theirs in the limit of infinite stretching. We begin with the expression for the classical free energy, eq 38. In the limit $\beta \to \infty$, the free energy becomes

$$\frac{F_{\mathrm{cl}}}{\beta} = -\frac{1}{2}\int_0^\infty \mathrm{d}z\, \phi^2(z) + \int_0^\infty \mathrm{d}z_0\, g(z_0) \int_0^{z_0} |e(z,z_0)| + \frac{\phi(z)}{|e(z,z_0)|}\,\mathrm{d}z \tag{A1}$$

Variation with respect to e leads again to eq 41. In contrast, variation with respect to $g(z_0)$ does not lead to an equation determining $g(z_0)$, since it appears only linearly. In fact, the resulting equation can always be solved, since the generating functional contains a term proportional to the undetermined Lagrange multiplier λ; see eq 40. It follows that the end-point distribution is only determined by its relation to the density, eq 33. However, as we recall below, the density profile is completely determined to be parabolic by the fact that the end points are unstretched in the limit $\beta \to \infty$, as shown by eq 42.

1. Parabolic Density Profile. When the end points are unstretched, the stretching function e of eq 41 reduces to

$$e^2(z,z_0) = \phi(z) - \phi(z_0) \tag{A2}$$

so that the equal-length constraint, eq 39, can be written as

$$\int_0^{z_0} \frac{\mathrm{d}z}{[\phi(z) - \phi(z_0)]^{1/2}} = 1 \tag{A3}$$

Changing the integration variable from z to ϕ, and using the notations $\phi_0 = \phi(0)$ and $\phi_{z_0} = \phi(z_0)$, one obtains

$$\int_{\phi_0}^{\phi_{z_0}} \frac{\mathrm{d}\phi}{\phi'(\phi)[\phi - \phi_{z_0}]^{1/2}} \tag{A4}$$

where $\phi'(\phi) = (\mathrm{d}z(\phi)/\mathrm{d}\phi)^{-1}$ and $z(\phi)$ is the inverse function of $\phi(z)$. This equation is an example of an Abel equation, which can be solved as follows. First one multiplies both sides by $\int_{\phi_z}^{\phi_0} \mathrm{d}\phi_{z_0}/(\phi_{z_0} - \phi_z)^{1/2}$ and obtains

$$\begin{aligned}\int_{\phi_z}^{\phi_0} \frac{\mathrm{d}\phi_{z_0}}{[\phi_{z_0} - \phi_z]^{1/2}} &= \int_{\phi_z}^{\phi_0} \frac{\mathrm{d}\phi_{z_0}}{[\phi_{z_0} - \phi_z]^{1/2}} \int_{\phi_0}^{\phi_{z_0}} \frac{\mathrm{d}\phi}{\phi'(\phi)[\phi - \phi_{z_0}]^{1/2}} \\ &= \int_{\phi_z}^{\phi_0} \frac{\mathrm{d}\phi}{\phi'(\phi)} \int_{\phi_z}^{\phi} \frac{\mathrm{d}\phi_{z_0}}{[\phi_{z_0} - \phi_z]^{1/2}[\phi - \phi_{z_0}]^{1/2}} \\ &= \pi \int_{\phi_z}^{\phi_0} \frac{\mathrm{d}\phi}{\phi'(\phi)}\end{aligned} \tag{A5}$$

The integral on the left can be carried out so that eq A5 gives

$$2[\phi_0 - \phi_z]^{1/2} = \pi \int_{\phi_z}^{\phi_0} \frac{\mathrm{d}\phi}{\phi'(\phi_z)} \tag{A6}$$

Taking a derivative with respect to ϕ_z on both sides, one obtains a differential equation for $\phi(z)$

$$\frac{\mathrm{d}\phi(z)}{\mathrm{d}z} = \pi\sqrt{\phi_0 - \phi(z)} \tag{A7}$$

This equation can be solved by separation of variables and finally gives, together with the boundary condition $\phi(0) = \phi_0$, the solution

$$\phi(z) = \phi_0 - \frac{\pi^2}{4} z^2 \tag{A8}$$

It is this solution that has been plotted in Figures 1a and 5a as a heavy broken line. The normalization condition for ϕ, eq 15, determines the density at the wall to be

$$\phi_0 = \left(\frac{3\pi}{4}\right)^{2/3} \tag{A9}$$

The height of the brush, z_{m}, beyond which the density is identically zero, is then

$$z_{\mathrm{m}} = \left(\frac{6}{\pi^2}\right)^{1/3} \simeq 0.8471 \tag{A10}$$

2. End-Point Distribution. As noted above, in the infinite-stretching limit, the end-point distribution is only determined via its relation to the density, eq 33. With the stretching function given in eq A2, this integral equation becomes

$$\phi(z) = \int_z^{z_m} \frac{g(z_0)\,dz_0}{[\phi(z) - \phi(z_0)]^{1/2}}$$

$$= \frac{2}{\pi}\int_z^{\infty} \frac{g(z_0)\,dz_0}{[z_0^2 - z^2]^{1/2}} \tag{A11}$$

where, in the last step, we used the result for the density profile from the previous section. With new variables $y_0 = z_m^2 - z_0^2$ and $y = z_m^2 - z^2$, this integral equation attains the form of an inhomogeneous Abel equation

$$\phi(\sqrt{z_m^2 - y}) = \frac{1}{\pi}\int_0^y dy_0 \frac{g(\sqrt{z_m^2 - y_0})/\sqrt{z_m^2 - y_0}}{(y - y_0)^{1/2}} \tag{A12}$$

We use the same procedure as in the last section and compose both sides of eq A12 with the integral operator $\int_0^x dy/(x - y)^{1/2}$, leading to

$$\int_0^x dy \frac{\phi(\sqrt{z_m^2 - y})}{\sqrt{x - y}}$$

$$= \frac{1}{\pi}\int_0^x \frac{dy}{\sqrt{x - y}}\int_0^y dy_0 \frac{g(\sqrt{z_m^2 - y_0})/\sqrt{z_m^2 - y_0}}{(y - y_0)^{1/2}}$$

$$= \frac{1}{\pi}\int_0^x dy_0 \frac{g(\sqrt{z_m^2 - y_0})}{\sqrt{z_m^2 - y_0}}\int_{y_0}^x \frac{dy}{(x - y)^{1/2}(y - y_0)^{1/2}}$$

$$= \int_0^x dy_0 \frac{g(\sqrt{z_m^2 - y_0})}{\sqrt{z_m^2 - y_0}} \tag{A13}$$

Taking a derivative with respect to x on both sides, one obtains

$$\frac{\phi(z_m)}{\sqrt{x}} - \frac{1}{2}\int_0^x dy \frac{\phi'(\sqrt{z_m^2 - y})}{(z_m^2 - y)^{1/2}(x - y)^{1/2}} = \frac{g(\sqrt{z_m^2 - x})}{(z_m^2 - x)^{1/2}} \tag{A14}$$

Choosing $x = z_m^2 - z_0^2$ and changing y back to $y = z_m^2 - z^2$ one arrives at

$$g(z_0) = \frac{\phi(z_m)z_0}{(z_m^2 - z_0^2)^{1/2}} - z_0\int_{z_0}^{z_m} dz \frac{\phi'(z)}{(z^2 - z_0^2)^{1/2}} \tag{A15}$$

Using the parabolic result for $\phi(z)$ and performing the integral in eq A15, one obtains the result of Zhulina et al. and Milner, Witten, and Cates

$$g(z_0) = \frac{\pi^2}{2} z_0 (z_m^2 - z_0^2)^{1/2} \tag{A16}$$

whose integral is normalized to unity. This is the asymptotic function which we plotted in Figure 1b and 5b as heavy broken lines.

With the infinite β results for $\phi(z)$, eq A19, and $g(z_0)$, eq A16, the limiting form of the classical free energy, eq 38, is

$$\frac{F_{cl}}{\beta} = (6\pi)^{2/3}3/20 + \frac{1}{\beta}(2\ln[6\pi] - 5)/3 \simeq 1.0624 + \frac{0.2910}{\beta}$$

Appendix B: Noninteracting Grafted Polymers

If one neglects the interactions between polymers, the segment probability amplitudes eqs 22 and 23 are solutions of the free diffusion equation

$$\frac{\partial q(z,t)}{\partial t} = \frac{1}{4\beta}\frac{\partial^2 q(z,t)}{\partial z^2} \tag{B1}$$

$$\frac{-\partial q^\dagger(z,t)}{\partial t} = \frac{1}{4\beta}\frac{\partial^2 q^\dagger(z,t)}{\partial z^2} \tag{B2}$$

With the initial conditions for a polymer fixed with one end to the impenetrable wall and with the other end at a distance z_0 from this wall, $q(z,1) = \delta(z - z_0)$ and $q^\dagger(z,0) = \delta(z)$, the solutions can be calculated using the method of images. The solution of q is given by

$$q(z,t) = \sqrt{\frac{\beta}{\pi t}}\left[\exp\left\{-\frac{\beta(z - z_0)^2}{t}\right\} - \exp\left\{-\frac{\beta(z + z_0)^2}{t}\right\}\right] \tag{B3}$$

while the normalized solution for $q^\dagger$ is

$$\frac{q^\dagger(z,t)}{\int_0^\infty dz\, q^\dagger(z,t)} = \frac{2\beta}{1 - t} z \exp\left\{-\frac{\beta}{1 - t}z^2\right\} \tag{B4}$$

These solutions describe the polymer statistics completely. The average paths are defined by

$$\langle z(t,z_0)\rangle = \frac{\int_0^\infty z q(z,t)|_{z_0} q^\dagger(z,t)}{\int_0^\infty dz'\, q(z',t)|_{z_0} q^\dagger(z',t)} \tag{B5}$$

and can be calculated exactly, leading to

$$\langle z(t,z_0)\rangle = \frac{z_0 t}{\sqrt{\pi}}\gamma[1/2,\beta z_0^2 t/(1 - t)] - 2\sqrt{\frac{t(1 - t)}{\beta\pi}}\gamma[1,\beta z_0^2 t/(1 - t)] + \frac{1 - t}{z_0\beta\sqrt{\pi}}\gamma[3/2,\beta z_0^2 t/(1 - t)] + 2\sqrt{\frac{t(1 - t)}{\beta\pi}} \tag{B6}$$

where γ is the incomplete γ function.

References and Notes

(1) Auroy, P.; Auvray, L.; Leger, L. *Macromolecules* **1991**, *24*, 2523.
(2) For an overview over stretching effects in melts and solvent systems see: Halperin, A.; Tirrell, M.; Lodge, T. P. *Adv. Polym. Sci.* **1992**, *100*.
(3) Alexander, S. *J. Phys. (Paris)* **1977**, *38*, 983.
(4) de Gennes, P.-G. *Macromolecules* **1980**, *13*, 1069.
(5) Milner, S. T.; Witten, T. A.; Cates, M. E. *Europhys. Lett.* **1988**, *5*, 413; *Macromolecules* **1988**, *21*, 2610.
(6) Skvortsov, A. M.; Gorbunov, A. A.; Pavlushkov, V. A.; Zhulina, E. B.; Borisov, O. V.; Priamitsyn, V. A. *Polym. Sci. USSR* **1988**, *30*, 1706. Zhulina, E. B.; Priamitsyn, V. A.; Borisov,

O. V. *Polym. Sci. USSR* **1989**, *31*, 205. Zhulina, E. B.; Borisov, O. V.; Priamitsyn, V. A. *J. Colloid Interface Sci.* **1990**, *137*, 495.
(7) Semenov, A. N. *Sov. Phys. JETP* **1985**, *61*, 733.
(8) Orland, H.; Schick, M. *Macromolecules* **1996**, *29*, 713.
(9) Scheutjens, J. M. H. M.; Fleer, G. J. *J. Phys. Chem.* **1979**, *83*, 1619; **1980**, *84*, 178.
(10) Fleer, G. J.; Cohen Stuart, M. A.; Scheutjens, J. M. H. M.; Cosgrove, T.; Vincent, B. *Polymers at Interfaces*; Chapman and Hall: London 1993.
(11) Netz, R. R.; Schick, M. *Europhys. Lett.* **1997**, *38*, 37.
(12) Birshtein, T. M.; Zhulina, E. B. *Polymer* **1984**, *25*, 1453.
(13) Murat, M.; Grest, G. S. *Macromolecules* **1989**, *22*, 4054. Grest, G. S.; Murat, M. *Macromolecules* **1993**, *26*, 3108.
(14) Cosgrove, T.; Heath, T.; van Lent, B.; Leermakers, F.; Scheutjens, J. *Macromolecules* **1987**, *20*, 1692.
(15) Chakrabarti, A.; Toral, R. *Macromolecules* **1990**, *23*, 2016.
(16) Lai, P.-Y. Zhulina, E. B. *J. Phys. II Fr.* **1992**, *2*, 547.
(17) Lai, P.-Y.; Binder, K. *J. Chem. Phys.* **1991**, *95*, 9288; **1992**, *97*, 586.
(18) This problem does not occur for the semiflexible polymer model, whose extreme-stretching limit is well behaved for single polymers[19] and for polymer melts.[20] Note that the classical theory can also be formulated for semiflexible polymers.[21]
(19) Marko, J. F.; Siggia, E. D. *Macromolecules* **1995**, *28*, 8759.
(20) Netz, R. R.; Schick, M. *Phys. Rev. Lett.* **1996**, *77*, 302.
(21) Netz, R. R. To be published.
(22) Carignano, M. A.; Szleifer, I. *J. Chem. Phys.* **1993**, *98*, 5006.
(23) Martin, J. I.; Wang, Z.-G. *J. Phys. Chem.* **1995**, *99*, 2833.
(24) We are indebted to H. Orland for this observation.
(25) Milner, S. T. *J. Chem. Soc., Faraday Trans.* **1990**, *86*, 1349.
(26) Wijmans, C. M.; Scheutjens, J. M. H. M.; Zhulina, E. B. *Macromolecules* **1992**, *25*, 2657.
(27) Helfand, E. *J. Chem. Phys.* **1975**, *62*, 999.
(28) Johner, A.; Joanny, J. F. *J. Chem. Phys.* **1993**, *98*, 1647.
(29) Matsen, M. W. *J. Chem. Phys.* **1995**, *102*, 3884. Matsen, M. W.; Bates, F. S. *Macromolecules* **1995**, *28*, 8884.
(30) Henceforth we will drop the subscript "cl" on the density, ϕ, and end-point distribution, $g(z_0)$.
(31) Witten, T. A.; Leibler, L.; Pincus, P. A. *Macromolecules* **1990**, *23*, 824.
(32) Venema, P.; Odjik, T. *J. Phys. Chem.* **1992**, *96*, 3922.
(33) Subramanian, G.; Williams, D. R. M.; Pincus, P. A. *Europhys. Lett.* **1995**, *29*, 285.
(34) Pincus, P. A. *Macromolecules* **1976**, *9*, 386.

MA9717505